JOURNAL OF GEOPHYSICAL RESEARCH, VOL. 100, NO. A12, PAGES 23,515–23,522, DECEMBER 1, 1995

Measurement of the energy spectra of cosmic ray electron component and protons at ground level

R. L. Golden,[1,2] S. A. Stephens,[3] S. J. Stochaj,[1] W. R. Webber,[1] M. T. Brunetti,[4] A. Codino,[4] C. Grimani,[4] M. Menichelli,[4] I. Salvatori,[4] M. P. De Pascale,[5] A. Morselli,[5] P. Picozza,[5] G. Basini,[6] F. Bongiorno,[6,7] F. M. Brancaccio,[6] M. Ricci,[6] J. F. Ormes,[8] R. E. Streitmatter,[8] P. Papini,[9] S. Piccardi,[9] and P. Spillantini[9]

Abstract. Using a superconducting magnet spectrometer, we have measured the energy spectra of electrons, positrons, and protons at ground level at an atmospheric depth of 945 g/cm^2. The differential energy spectrum of the electron component has been determined in the momentum interval between 0.1 and 2.0 GeV/c. This spectrum can be described by two power laws, one below 600 MeV with a spectral index of -1.8 ± 0.1 and the other above this energy with an index of -2.9 ± 0.2. The absolute flux values measured here are not in agreement with the earlier results. The fraction of positrons varies from a value of 0.45 at 200 MeV to about 0.5 above 1 GeV, which is consistent with the theoretical expectation. The momentum dependence of the e/μ ratio in the region between 0.25 and 2.0 GeV/c is proportional to $p^{-2.2}$, and it appears that the soft component of the ionizing radiation might dominate at ground level at kinetic energies below about 70 MeV. The proton energy spectrum has been determined as a power law in kinetic energy between 2.9 and 19.1 GeV with a spectral index of -2.66 ± 0.26. The p/μ ratio obtained from this experiment seems to have a steeper momentum dependence than from previous experiments.

Introduction

Cosmic radiation observed at ground level is the end product of the propagation of primary cosmic rays in the overlying atmosphere. This radiation consists mainly of weakly interacting muons. Most of the protons at ground level are the surviving fraction of the primary nucleons after their energy has been degraded during the traversal of nearly 11 interaction mean free paths of matter in the atmosphere. The surviving number of protons and their spectral shape depend upon the charge exchange process and the distribution of inelasticity during nuclear interactions. On the other hand, electrons at ground level are due to the electromagnetic cascade processes resulting from the interaction of primary and secondary cosmic rays in the atmosphere. A reasonable fraction of them at higher energies also come from the decay of muons [*Daniel and Stephens*, 1974]. An accurate determination of the spectra of these components gives information on the physical processes involved in the propagation and on the composition of the primary component. It also provides a standard source for the calibration of detector systems, which are developed for the study of primary cosmic rays.

The energy spectrum and the charge ratio of muons at sea level have been measured extensively in the past over a wide range of energies. However, only a few attempts have been made to measure the spectra of electrons and protons at sea level. None of the instruments used in these studies had the capability to detect all these components in a single experiment. In the same manner, many theoretical estimates have been made in the past to explain the muon observations [e.g., *Badhwar et al.*, 1977; *Lipari*, 1993], while only a few estimates have been made of the spectrum of protons deep in the atmosphere [e.g., *Yash Pal and Peters*, 1964; *Barber et al.*, 1980]. It may be noted that for the propagation of the electromagnetic components only one detailed calculation exists which covers the entire atmosphere [*Daniel and Stephens*, 1974]. These estimates imply the close relationship of theoretical attempts to the availability of observational results. A proper comparison between observations and theory is essential to enhance our understanding of the effect of complex physical processes in the atmosphere. In the experiment described here, we used a superconducting magnet spectrometer, which was also deployed to study the primary and secondary cosmic rays at the top of the atmosphere [*Papini et al.*, 1993; *Golden et al.*, 1994] and the muon component during the ascent of the balloon [*De Pascale et al.*, 1993; *Grimani et al.*, 1993; R. Bellotti et al., manuscript in preparation, 1995]. Details of this experiment and the experimental setup are described by *De Pascale et al.* [1993]. A portion of this description is repeated here and in the

[1]Particle Astrophysics Laboratory, New Mexico State University, Las Cruces.
[2]Deceased April 7, 1995.
[3]Tata Institute of Fundamental Research, Bombay, India.
[4]Dipartimento di Fisica dell' Università and Sezione Istituto Nazionale di Fisica Nucleare di Perugia, Perugia, Italy.
[5]Dipartimento di Fisica dell' Università and Sezione Istituto Nazionale di Fisica Nucleare di Roma II, Rome, Italy.
[6]INFN Laboratori Nazionali di Frascati, Frascati, Italy.
[7]Dipartimento di Electronica, III Università di Roma, Rome, Italy.
[8]NASA Goddard Space Flight Center, Greenbelt, Maryland.
[9]Dipartimento di Fisica dell' Università and Sezione INFN di Firenze, Firenze, Italy.

Paper number 95JA02449.
0148-0227/95/95JA-02449$05.00

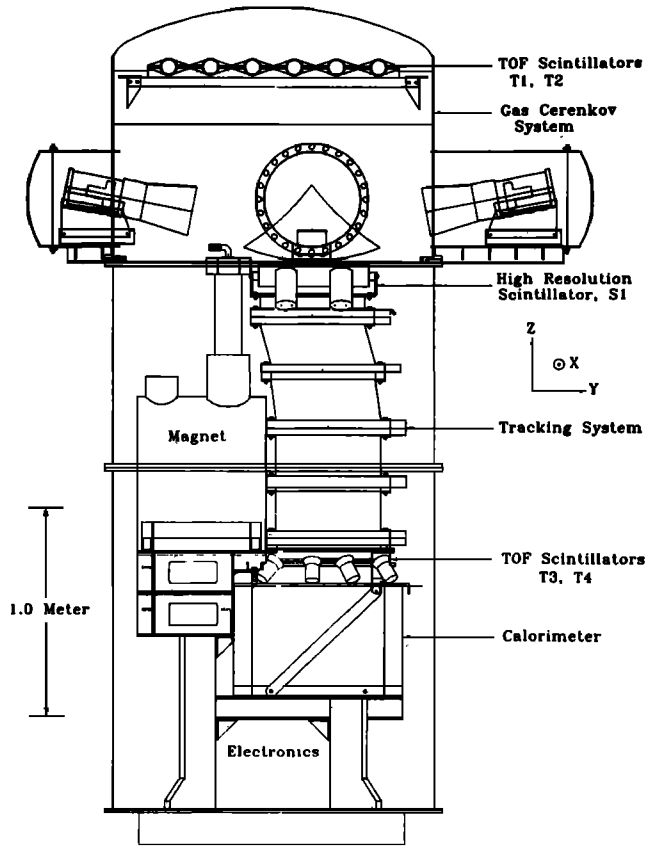

Figure 1. A schematic diagram of the magnet spectrometer used in this experiment [from *De Pascale et al.*, 1993].

following section for the convenience of the reader. The data used here were gathered during a ground run of this Matter Antimatter Superconducting magnet Spectrometer (MASS) apparatus on August 30, 1989, at Prince Albert, Saskatchewan, Canada. This location is at latitude 53°N and longitude 106°W and is 600 m above sea level. Preliminary results from this experiment were reported earlier [*Basini et al.*, 1993], and in this paper we present the final results. We compare our observed spectra on proton and electron components with other experimental results and with theoretical calculations.

Experimental Setup

The MASS apparatus used for this experiment has been described in detail elsewhere [*Golden et al.*, 1991; *De Pascale et al.*, 1993]. We summarize here the basic detector elements of this instrument, which was designed as a balloon-borne magnet spectrometer for cosmic ray studies. The instrument is shown in Figure 1 and has the following detectors. (1) Eight multiwire proportional chambers (MWPC) were used to record the particle trajectory in the magnetic field. (2) A time of flight (TOF) device having two planes, each with two layers of scintillators (T1, T2) and (T3, T4) separated by a distance of 2.4 m, provided information on the particle direction and velocity. (3) TOF scintillators and an additional high-resolution scintillator S1 were used for the measurement of particle charge. (4) A gas Cherenkov counter filled with an equal mixture of Freon 12 and Freon 22 by volume, giving it a threshold Lorentz factor of 23 was placed just below the top plane of the TOF. (5) A calorimeter of size 50 cm × 50 cm × 40 cm (depth) and weight 418 kg was kept just below the scintillator T4. It consisted of 40 layers of 64 brass streamer tubes in which alternate layers were arranged perpendicular to each other. The walls of the streamer tubes served as the passive material, and the calorimeter had an effective depth of 7.33 radiation lengths, which is equivalent to a 0.75 interaction mean free path for protons.

The superconducting magnet was operated at 120 A current, producing a magnetic field of 10 to 40 kGauss in the MWPC region. The spectrometer resolution was such that the maximum detectable rigidity (R is momentum/charge) was found to be 118 GV/c. Signals from the MWPC were fed to the delay lines and were digitized, from which arrival times at each end of the delay lines were measured. The sum of the delay line readout times was required to be equal to the total delay of the line in order for the data to be accepted. Signals from all five scintillator layers and from the Cherenkov detector were pulse height analyzed. The calorimeter image data were also gathered in digital form. The trigger for an event was a coincidence between T1, T2, T3, and T4. The performance of this detector system is described in detail by *Golden et al.* [1991].

Analyses of Data

Selection of Events

The selection criteria used in this analysis are shown in Table 1. We required the event to have a good trajectory in the spectrometer, and the criteria used for the selection of events (tests 1 to 4) are the same as those obtained by *Golden et al.* [1991]. After selecting singly ionizing particles using signals

Table 1. Selection Criteria

Test	Description
1	a minimum of five x axis and three y axis MWPC measurements should have good time sum
2	at least one of each pairs of the top, middle, and bottom X MWPC and the bottom Y MWPC must be usable
3	the least squares fit to the reconstructed track must satisfy $X_x^2 \leq 5$ and $X_y^2 \leq 7.5$
4	the deflection uncertainty should be ≤ 0.03
5	signal S from T1 and T2 should be $0.5I_o \leq S \leq 2.0I_o$
6a	Cherenkov signal should correspond to at least one photoelectron (for electrons)
6b	no Cherenkov signal (for protons)
7	the ratio of the total number of cell hits to those along the particle trajectory in the calorimeter should be ≥ 2.2

MWPC is multiwire proportional chambers.

from T1 and T2 (test 5), we made use of the signals from the Cherenkov detector and calorimeter for further analysis to distinguish electron and proton events. In the case of electron events we required that it was accompanied by a Cherenkov signal corresponding to >1 photo electron (test 6a). The accidental rate for such signals was only 5×10^{-4} [*Golden et al.*, 1994]. Below 500 MeV, where the number of electromagnetic shower particles is small, the above criterion was found to be sufficient to distinguish an electron from muons efficiently. As a consequence, it was not essential to include calorimeter data for this analysis, and thus we were able to increase the available geometry for the low energy bin by requiring that the event should pass through only the middle layer of the calorimeter. A visual examination of a sample of events close to 500 MeV, which is within the full geometry of calorimeter, showed that all of the events exhibited electromagnetic cascade development in the calorimeter.

As the energy of the event slowly approached the Cherenkov threshold for muons (2.4 GeV), a small fraction of muons started showing Cherenkov signal. Therefore we found it useful to include additional calorimeter constraint to identify electrons. The initial selection of events above 500 MeV was made similar to that of *Golden et al.* [1994], in which it was required that the trajectory was well inside the calorimeter, 3 cm from the sides. We have chosen a broad energy interval between 500 MeV and 2 GeV in order to have sufficient statistics to carry out the following analysis. Since muons are weakly interacting particles, we expect them to produce a signal only along their trajectory in the calorimeter, while electrons are expected to produce multiple hits laterally also. Therefore we examined the ratio R_h of the total number of cell hits recorded by an event in the calorimeter to those along the trajectory in the above energy range. We have shown in Figure 2 the distribution of these events as a function of R_h. Notice that this distribution has a peak close to $R_h = 1$ and has a tail with a cutoff at 1.8. These events are clearly the muons in the sample. The remainder of the events in Figure 2 shows an extended distribution starting from a value of 2.4, and these are mostly due to electron showers. Therefore we set an additional criterion that an electron event requires to satisfy $R_h < 2.2$ (test 7). The solid curve shown in Figure 2 is the Gaussian fit to the data below $R_h = 2.2$, which peaks at $R_h = 1.1$. The width of this distribution indicates the probability of random hits in the calorimeter volume. We have also shown in Figure 2 the distribution of R_h from $R_h = 2.0$ to 24.0. This distribution clearly reflects the energy spectrum of the electrons.

Because of the spurious hits in the calorimeter, some muons would be identified as electrons by this criterion, and we estimated that 4% of the selected sample would contain muons. Figure 2 also indicates that about 1% of the electrons would have $R_h < 2.0$. Thus we found that the effective contamination in our sample of electrons is only about 3%, and this information was used for correcting the data above 500 MeV. The calorimeter criterion (test 7) was not sufficient to identify electrons unambiguously. Above the Cherenkov threshold for muons the requirement of a Cherenkov signal (test 6a) becomes ineffective as a characteristic of an electron event. Therefore we have restricted the maximum energy to 2 GeV for electrons. A total of 437 e^- and 343 e^+ were identified in the energy region from 100 MeV to 2 GeV for further analysis.

In the case of protons we selected singly ionizing events with positive curvature and with no Cherenkov signal (test 6b). We also required $R_h > 2.2$ (test 7) in order to select proton interaction in the calorimeter. Thus the event selection required all the tests shown in Table 1, except test 6a. The selected events were examined visually for interaction vertex to confirm that the event is due to a proton. Proton selection was made in the restricted geometry as in the case of electrons above 500 MeV. A total of 69 protons were identified. This number was corrected for noninteracting ones in the calorimeter. We need to examine possible vetoing of interacting protons by MWPC due to multiple tracks, resulting from the secondary particles going backward from the interaction. For this purpose we divided the calorimeter into two equal upper and lower sectors. We found 41 interactions in the upper sector, and on this basis we expected 28 interactions in the lower sector and found 30 ± 5.5. From this good agreement between the expectation and the observation we conclude that there is no loss of events due to self-vetoing.

Collecting Power of the Instrument

We have calculated the geometric factor (GF) for this instrument similar to that described by *De Pascale et al.* [1993].

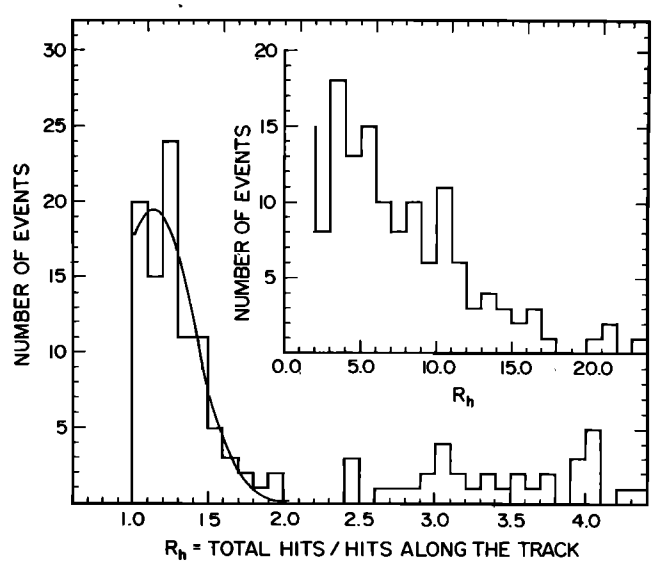

Figure 2. The distribution of the ratio of total number of cell hits in the calorimeter to the number of cell hits along the trajectory of the event.

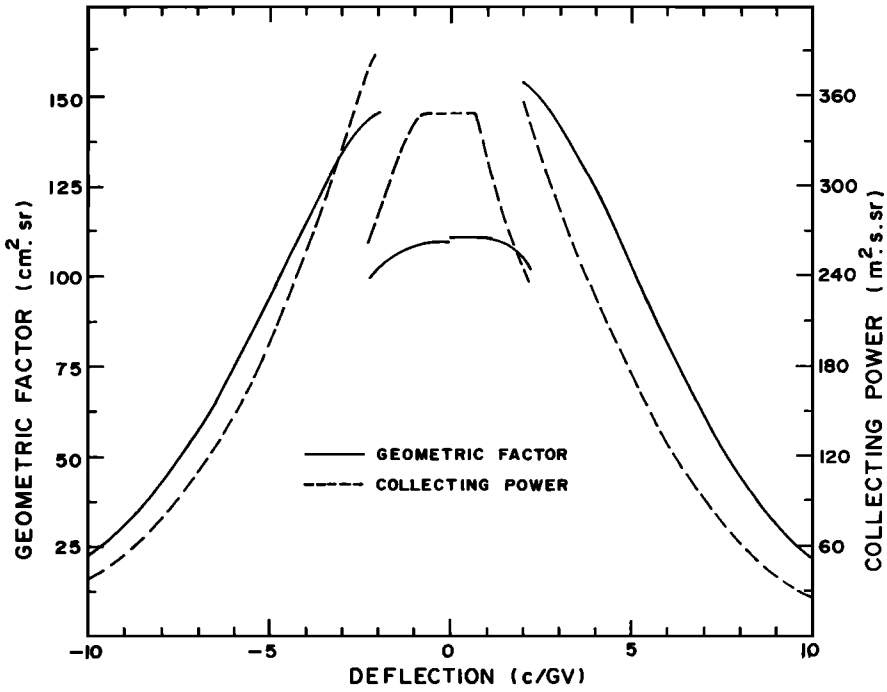

Figure 3. A plot of the calculated geometric factor and the collecting power of the instrument as a function of deflection for electrons. The discontinuity results from the different criteria used for the selection of electrons as described in the text.

For electrons <500 MeV we required the particle to enter the instrument from T1 scintillator and leave by the middle layer of the calorimeter. Further, the particle should traverse the sensitive area of all the detectors including the Cherenkov detector. In the case of electrons >500 MeV and for protons it was required that the particle trajectory leaves from the bottom layer of the calorimeter and intersects the central plane of the calorimeter at a distance >3 cm from all sides. This restriction resulted in the decrease of the GF by 30%. The solid line in Figure 3 shows the calculated value of GF as a function of the deflection (d = 1/rigidity) of the particle. It is seen that GF decreases as the absolute deflection increases. Notice the sudden increase in GF at d = 2.0 c/GV due to the change in the selection criterion. In the case of protons the GF is 110.5 cm^2 sr.

In order to estimate the collecting power of the instrument, one needs to know the detector efficiency relating to each set of tests applied to the events. These are described below:

1. Spectrometer efficiency e_s, that is, the overall efficiency of the spectrometer for particles satisfying test 1 to test 4, was found to be 0.69 ± 0.01 for R > 4 GV/c. *De Pascale et al.* [1993] showed that this efficiency decreased with decreasing rigidity and was found to be dependent on the sign of the charge. We have extrapolated this dependence by a power law in rigidity below 0.2 GV/c using the experimentally determined efficiencies below 0.6 GV/c. We have included the errors in the extrapolation of the efficiency in calculating the flux values.

2. Calorimeter efficiency e_c, that is, the efficiency of the calorimeter to detect a singly charged particle passing through it, was found to be 100% even though the individual cell efficiency was 82%. We have mentioned that application of test 7 for events >500 MeV resulted in a misidentification of a small fraction of muons and electrons. This amounts to an overestimate of the electron number by a factor 1.03 ± 0.01.

3. Scintillator efficiency e_{sc}, that is, the rejection of events due to the criteria used for the selection of singly charged particles by test 5, was estimated by examining the distribution of events in the high-resolution scintillator S1. It was found that the efficiency by which particles satisfied test 5 is 0.96 with negligible error.

4. Other efficiency e_o, that is, a combination of various other additional efficiencies. We found a tape reading efficiency of 0.93, which is due to the disk-write time of the ground computer being larger than the buffering capability of the input interface while transcripting the analog tapes. In addition, the dead time resulted in an efficiency of 0.98 for recording events. We also noticed an inefficiency in the trigger rate, partly because of the observed position dependent variation of the pulse height in T1, T2, T3, and T4 and partly due to these scintillator planes being segmented. This was experimentally determined and found to be 0.82 ± 0.01. In the case of electrons some are lost because of the materialization of the bremsstrahlung photons in the spectrometer. It is estimated that in the energy region of interest here, this effect decreases the efficiency of the spectrometer by a factor 0.93. By combining these efficiencies the value of e_o is 0.70 ± 0.01 for electrons and 0.75 ± 0.01 for protons. There could be a possible systematic uncertainty of about 10%.

Now the collecting power (CP) of the MASS instrument is defined as the product of GF, e_s, e_c, e_{sc}, e_o and the total time of observation. The data analyzed here correspond to a total observation time of 70,340 s. The dashed curve in Figure 3 shows the estimated value of CP as a function of deflection for electrons. The value of CP varies from 347.3 (m^2 sr s) for R > 5 GV/c to 280.0 at R = 0.5 GV/c for electrons. Because of the change of criteria below 0.5 GV/c, CP becomes high and decreases from 382.4 (m^2 sr s) at 0.5 GV/c to 38.2 at 0.1 GV/c. Similarly, for the positrons the corresponding values are 348.2,

Table 2. Differential Flux of Electrons

Deflection Interval, c/GV	Median Energy, GeV	Observed Number of Electrons		Flux (Percent Error), el/(m^2 s sr GV/c)		$e^+/(e^+ + e^-)$, (Percent Error)
		Negative	Positive	Negative	Positive	
0.5–1.0	1.393	20	20	0.0494 (22)	0.0505 (22)	0.504 (16)
1.0–1.5	0.927	25	29	0.201 (20)	0.251 (19)	0.552 (15)
1.5–2.0	0.658	30	28	0.535 (18)	0.573 (19)	0.518 (13)
2.0–2.4	0.521	48	32	1.445 (14)	1.108 (18)	0.430 (9)
2.4–3.0	0.426	57	47	1.920 (13)	1.783 (15)	0.484 (9)
3.0–3.6	0.347	52	38	2.984 (14)	2.487 (17)	0.456 (9)
3.6–4.8	0.274	79	63	4.588 (12)	4.132 (13)	0.476 (8)
4.8–6.0	0.212	48	38	6.559 (15)	5.767 (17)	0.471 (12)
6.0–7.2	0.175	39	27	11.15 (17)	9.016 (20)	0.454 (14)
7.2–9.6	0.150	37	21	15.04 (20)	10.98 (27)	0.439 (18)

246.1, 340.0, and 29.4 (m^2 sr s), respectively. In the case of protons we need to consider the probability that the proton interacts inside the calorimeter, which is 0.528; the collecting power for protons above 1 GV/c is 196.5 (m^2 sr s). All the errors associated with above efficiencies are assumed to be independent of each other in evaluating the total error in the flux. As mentioned earlier, there could be possible systematic uncertainty of 10% in determining the absolute flux values. It should be emphasized that we have carried out a careful study of the energy dependence of the criteria for selecting the muon events.

Results

Electron Spectrum

The differential flux of electrons is calculated by using the observed number of electrons in a given energy bin and the collecting power of the MASS instrument. These flux values were then corrected for bremsstrahlung energy loss resulting from the traversal of 0.13 radiation length of matter in the instrument, using cascade theory to obtain the flux above the instrument. Table 2 gives these estimated flux values along with other relevant parameters. Table 2 gives the median energy, corresponding to the selected deflection bin, at the top of the instrument. The fraction of positrons in each bin is also shown. All the errors given in Table 2 include statistical and those associated with the efficiencies discussed earlier. Notice in Table 2 that at low energies, the errors associated with the efficiencies play an important role.

The energy spectrum of total electrons ($e^+ + e^-$) is plotted in Figure 4. The spectrum can be described by two power laws, one below about 600 MeV and one above this energy. The spectral index below 600 MeV is -1.8 ± 0.1, while above 600 MeV it is -2.9 ± 0.2. For a comparison, we have shown the measurements by *Beuermann and Wibberenz* [1968] at sea level, which has been corrected for the present altitude using an attenuation mean free path of 200 g/cm^2 [*Daniel and Stephens*, 1974]. Notice the disagreement between these two results. Our results are lower by about a factor 2.6 below 600 MeV, and this disagreement increases with increasing energy. At such large atmospheric depths the geographical location of the experiment does not play any role in modifying the spectrum [*Daniel and Stephens*, 1974], and hence this difference could be due to the experimental determination of electron detection efficiency. We believe that we have carefully determined this efficiency and our results are reliable, as we have more information available for each event to make a careful analysis. In Figure 4 we have also shown the theoretical estimate by *Daniel and Stephens* [1974] by a solid curve, which falls in between the two experimental results but closer to our spectrum. The calculated spectrum is about a factor of 1.4 higher than our results below 600 MeV, and this difference increases as the energy increases. However, if we consider only the spectral shape

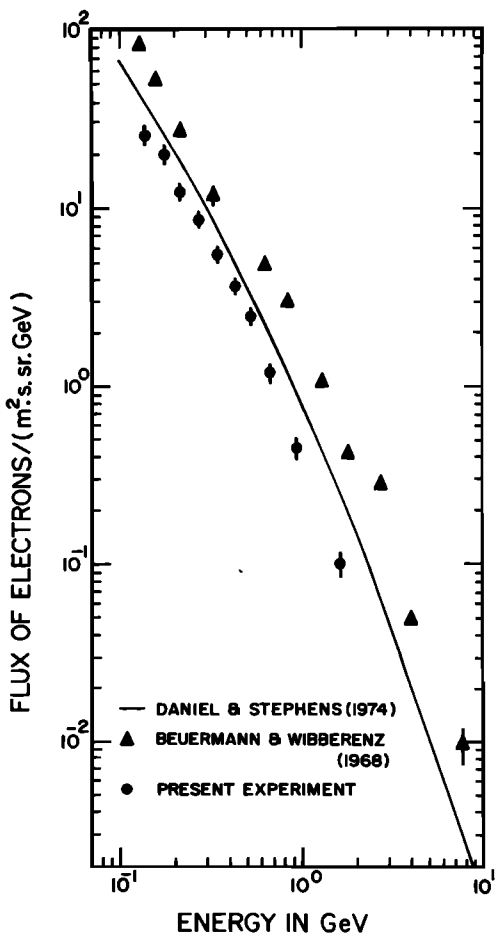

Figure 4. The differential flux of all electrons, both positive and negative, shown as a function of energy and compared with the theoretical expectation. The flux values of *Beuermann and Wibberenz* [1968] measured at sea level are corrected for attenuation to compare with the data at 945 g/cm^2.

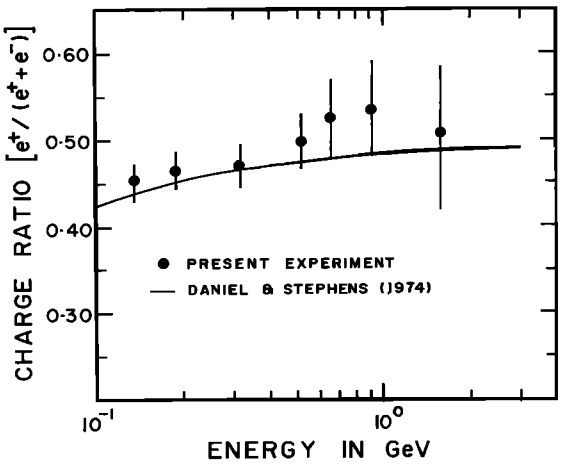

Figure 5. The fraction of positrons plotted as a function of energy and compared with the theoretical prediction.

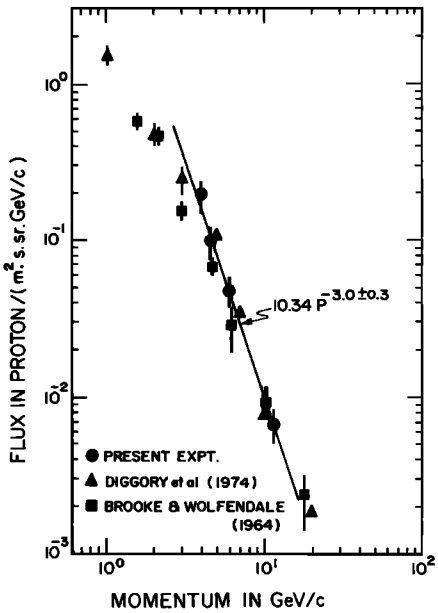

Figure 6. The flux of protons plotted as a function of momentum. The other flux values are corrected for the attenuation from sea level to 945 g/cm^2.

below 500 MeV, there is a very good agreement among all these results.

The observed fractions of positrons are also shown in Table 2. By summing up the energy intervals, we estimated the fraction from 0.12 GeV to 0.6 GeV to be 0.452 ± 0.017, while above 0.6 GeV it is 0.527 ± 0.044. From these estimates one clearly notices that the positron fraction slowly increases with energy. We have plotted the observed fraction as a function of energy in Figure 5. For comparison, we have shown by a solid curve the expected ratio at this depth from *Daniel and Stephens* [1974]. There is excellent agreement with the theoretical expectation. The general trend seen from Figure 5 and the observed values in the high- and the low-energy bins show that the low-energy electrons have some contribution from knock-on electrons to dilute the fraction of positrons, as expected. As the energy increases, the electrons consist mostly of the product of the electromagnetic cascade development in the atmosphere.

Proton Spectrum

The collecting power of the instrument for selecting proton events is 372.4 m^2 sr s. Since noninteracting protons are lost in our sample, this collecting power reduces to 196.5 m^2 sr s as the mean depth of this calorimeter is 0.75 interaction length for protons. We have shown in Table 3 the information on the proton flux analysis, that is, the median value of the momentum and kinetic energy of the deflection intervals. The number of observed interactions is also given as are the differential fluxes in momentum and in energy. The estimated proton flux values are plotted in Figure 6. This spectrum can be represented by a power law in momentum with a spectral slope of −3.0 ± 0.3 and in kinetic energy as

$$J(E) = 3.7E^{-2.66\pm0.26} \text{ proton/(m}^2 \text{ sr s GeV)}.$$

This spectral slope is in good agreement with that of the primary spectrum. For a comparison, we have shown the measured flux values at sea level [*Diggory et al.*, 1974; *Brooke and Wolfendale*, 1964]. These are multiplied by exp (85/120) to elevate to the present depth of 945 g/cm^2. Notice that our flux values are, in general, in agreement with the results from the earlier experiments within the uncertainities of the measurements. In the earlier experiments the flux values were obtained by normalizing the integral muon flux measured in the same experiment to some standard values, while we have determined the absolute flux values.

Ratios With Respect to Muons

The ratios of electrons to muons and protons to muons are plotted in Figure 7. In Figure 7 we have corrected the results of *Brooke and Wolfendale* [1964] for the attenuation of protons as described earlier and for that of muons using an attenuation mean free path of about 550 g/cm^2 (R. Bellotti et al., manuscript in preparation, 1995). It can be seen in Figure 7 that there is a noticeable difference between our results and those

Table 3. Differential Flux of Protons

Deflection Interval, c/GV	Median Momentum, GeV/c	Median Energy, GeV	Number of Events	Momentum Flux	Energy Flux	Error, %
0.5–0.14	11.64	10.74	17	6.73E−3	6.75E−3	24
0.14–0.20	5.96	5.10	20	4.76E−2	4.82E−2	22
0.20–0.24	4.56	3.72	16	9.81E−2	1.00E−1	25
0.24–0.27	3.93	3.10	18	1.95E−1	2.01E−1	24

Momentum flux in proton/(m^2 s sr GeV/c). Energy flux in proton/(m^2 s sr GeV). Read 6.73E−3 as 6.73 × 10^{-3}.

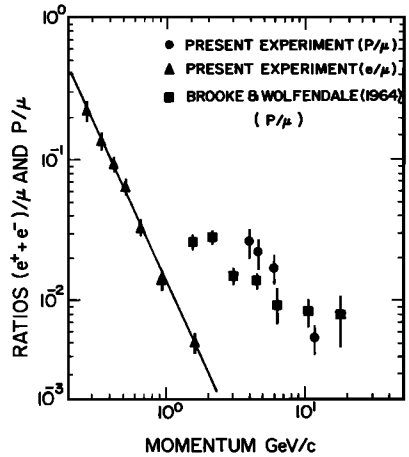

Figure 7. The ratios of electrons to muons and protons to muons plotted as a function of momentum. The ratios from other experiments are corrected for the attenuation from sea level to 945 g/cm^2.

of Brooke and Wolfendale; in particular, the p/μ ratio that we measured is steeper than in their results. Since our spectral slope is in agreement with the primary spectrum and the measured muon spectral shape flattens below about 30 GeV/c, we believe that our results are reliable. The muon spectrum that we obtained is in excellent agreement with other measurements and with theoretical expectations [see *De Pascale et al.*, 1993]. We conclude that the major source of this difference comes from the muon spectrum below 20 GeV/c, as measured by *Brooke and Wolfendale* [1964]. It will be interesting to extend the proton spectrum to lower energies to look for the effect of ionization, which flattens the spectrum below 2 GeV/c.

Figure 7 also shows the measured ratio of $e^+ + e^-$ to $\mu^+ + \mu^-$ as a function of momentum; the flux values of muons are taken from *De Pascale et al.* [1993]. Notice in Figure 7 that this ratio can be fitted by a power law in momentum P and can be represented as 0.0134 $P^{-2.2\pm0.1}$. It is expected that this strong dependence noticed at low energies would decrease as the energy increases. It is therefore interesting to extend the spectrum of electrons to higher energies to examine this. It is also clear from Figure 7 that the extrapolation of the power law dependence to lower energies indicates that the electron component would dominate the ionization radiation at kinetic energies below 70 MeV.

Summary and Discussions

1. The differential energy spectra of electrons and positrons have been measured for the first time near sea level in the energy region between 100 MeV and 2 GeV. The energy spectrum of all electrons can be approximated by two power law spectra, one above 600 MeV with a spectral index of -2.9 and one below this energy with an index of -1.8. Though the variation of the spectral shape is expected on the basis of the ionization loss, one needs to measure the shape accurately. It is essential that the energy spectrum is also extended to much higher energies.

2. The charge ratio of electrons in this energy range indicates that the fraction of positrons decreases with decreasing energy. This is again expected from theory as the contribution from knock-on electrons dominates at low energies. It is important that measurement is done with better statistical accuracy to determine the variation of charge ratio with energy over an extended energy region.

3. The present experimental results show that the absolute flux of electrons is much smaller than that measured by earlier experiments and the difference is more than a factor of 2. Though we believe that our results are very reliable, it is essential to measure this component with an instrument having a higher efficiency with greater rejection power against background events.

4. The ratio of electron to muon components at ground level as a function of energy has been measured for the first time with the same instrument. This ratio indicates that the soft component would dominate the ionizing radiation at ground level below 70 MeV. One needs to examine the implication of this result. However, it may be noted that the integral flux of this soft component is still only 1.9% of the muons at 140 MeV and it increases to 6% at 70 MeV.

5. We were also able to measure the energy spectrum of surviving protons in the energy region from 3 GeV to 19 GeV. The spectrum in this energy range can be represented by a power law with a spectral index of -2.7. There is general agreement with earlier results within the uncertainties of the measurements. One needs to measure this spectrum accurately over an extended energy region. The absolute spectrum of protons is very useful in understanding the influence of charge exchange probability and the distribution of inelasticity in the propagation of cosmic rays in the atmosphere.

6. There is general disagreement between the present results on proton to muon ratio and the earlier experiments. We believe that the difference seen is possibly due to the inaccurate determination of the spectra of those components in the previous experiment, especially the muon component. It is important that similar experiments are undertaken in the near future in which all components can be measured with high reliability.

Acknowledgments. This work was supported by NASA grant NAGW-110, the Istituto Nazionale di Fisica Nucleare, Italy, and the Agenzia Spaziale Italiana. We wish to record our special thanks to our technical support staff from NMSU and INFN.

The Editor thanks P. Király and T. K. Gaisser for their assistance in evaluating this paper.

References

Badhwar, G. D., S. A. Stephens, and R. L. Golden, Analytic representation of the proton-proton and proton-nucleus cross-sections and its application to the sea-level spectrum and charge ratio of muons, *Phys. Rev. D Part. Fields*, *15*, 820–831, 1977.

Barber, H. B., T. Bowen, D. A. Delise, E. W. Jenkins, R. M. Kalbah, and A. E. Pifer, Prediction and measurements of mass spectra of the charged nucleonic components of cosmic rays at mountain altitude, *Phys. Rev. D Part. Fields*, *22*, 2667–2687, 1980.

Basini, G., et al., Ground level observation of electrons, positrons and protons, *Proc. Int. Cosmic Ray Conf.*, *23rd*(3), 773–776, 1993.

Beuermann, K. P., and G. Wibberenz, Secondary spectra of electrons and photons in the atmosphere, *Can. J. Phys.*, *46*, S1034–S1037, 1968.

Brooke, G., and A. W. Wolfendale, The momentum spectrum of cosmic ray protons near sea level in the momentum range 0.6–150 GeV/c, *Proc. Phys. Soc. London*, *83*, 843–851, 1964.

Daniel, R. R., and S. A. Stephens, Cosmic ray produced electrons and gamma rays in the atmosphere, *Rev. Geophys.*, *12*, 233–257, 1974.

De Pascale, M. P., et al., Absolute spectrum and charge ratio of cosmic ray muons in the energy region from 0.2 GeV to 100 GeV at 600 m above sea level, *J. Geophys. Res.*, *98*, 3501–3511, 1993.

Diggory, I. S., J. R. Hook, I. A. Jenkins, and K. E. Turver, Momentum

spectra of nuclear active particles in the cosmic radiation at sea level, I, Experimental data, *J. Phys. A Math Nucl. Gen.*, *7*, 741–764, 1974.

Golden, R. L., et al., Performance of a balloon-borne magnet spectrometer for cosmic ray studies, *Nucl. Instrum. Methods Phys. Res., Sect. A*, *306*, 366–377, 1991.

Golden, R. L., et al., Observation of cosmic ray electrons and positrons using an imaging calorimeter, *Astrophys. J.*, *436*, 769–779, 1994.

Grimani, C., et al., Negative muon spectrum measurement at 5 g/cm^2, *Proc. Int. Conf. Cosmic Rays*, *23rd*(4), 507–510, 1993.

Lipari, P., Lepton spectra in the Earth's atmosphere, *Astropart. Phys.*, *1*, 195–227, 1993.

Papini, P., et al., Proton and helium spectra determination during the 1989 solar maximum, *Proc. Int. Conf. Cosmic Rays*, *23rd*(1), 579–582, 1993.

Yash Pal, and B. Peters, Meson production at high energies and the propagation of cosmic rays through the atmosphere, *Mat. Fys. Medd. K. Dan. Vidensk. Selsk.*, *33*(15), 1–55, 1964.

G. Basini, F. Bongiorno, F. M. Brancaccio, and M. Ricci, INFN-Laboratori Nazionali di Frascati, Via Enrico Fermi 40, I-00044 Frascati, Italy.

M. T. Brunetti, A. Codino, C. Grimani, M. Menichelli, and I. Salvatori, Dipartimento di Fisica dell' Università and Sezione INFN di Perugia, Via Elce di Sotto, I-06100 Perugia, Italy.

M. P. De Pascale, A. Morselli, and P. Picozza, Dipartimento di Fisica dell' Università and Sezione INFN di Roma II, Tor Vergata Via della Ricera Scientifica 1, I-00133 Rome, Italy.

J. F. Ormes and R. E. Streitmatter, NASA Goddard Space Flight Center, Greenbelt, MD 20771.

P. Papini, S. Piccardi, and P. Spillantini, Dipartimento di Fisica dell' Università and Sezione INFN di Firenze, Largo Enrico Fermi 2, I-50125 Firenze, Italy.

S. A. Stephens, Tata Institute of Fundamental Research, Homi Bhabha Road, Bombay 400 005, India.

S. J. Stochaj and W. R. Webber, Particle Astrophysics Laboratory, New Mexico State University, Las Cruces, NM 88003-0001.

(Received May 18, 1995; revised August 4, 1995;
accepted August 9, 1995.)